Electronic Supplementary Information

Organohydrogel Electrolyte with Solvated Structure Regulations for Highly Reversible Low-temperature Zinc Metal Battery

Feng Zhang, Mingchen Yang, Pengda Fang, Jiangtao Yu, Xinyu Ma, Yin Hu* and Feng Yan*

Jiangsu Engineering Laboratory of Novel Functional Polymeric Materials, Jiangsu Key Laboratory of Advanced Negative Carbon Technologies College of Chemistry, Suzhou Key Laboratory of Soft Material and New Energy, College of Chemistry, Chemical Engineering and Materials Science, Soochow University, Suzhou 215123, China.

* Correspondence to yinhu045@suda.edu.cn (Y. H.); or fyan@suda.edu.cn (F. Y.)

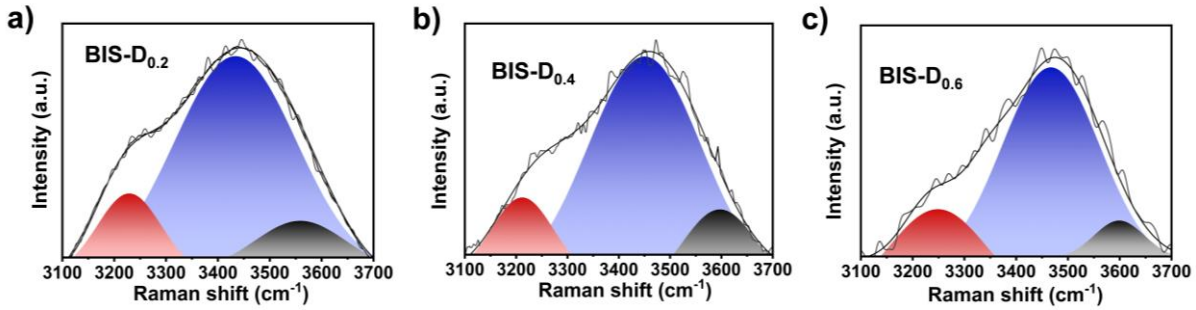

Figure S1. Raman spectra of fitted O-H stretching vibration in BIS-$D_{0.2}$, BIS-$D_{0.4}$ and BIS-$D_{0.6}$ electrolytes. The H-bonds between water molecules can be divided into strong, medium and weak H-bonds three states.

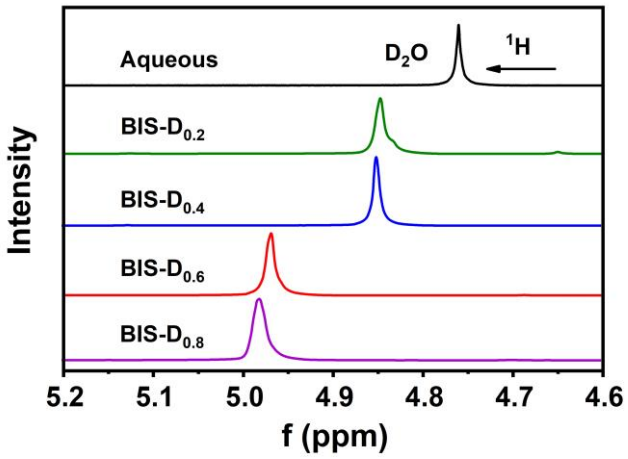

Figure S2. ^{1}H-NMR spectra of the bisolvent hybrid electrolytes.

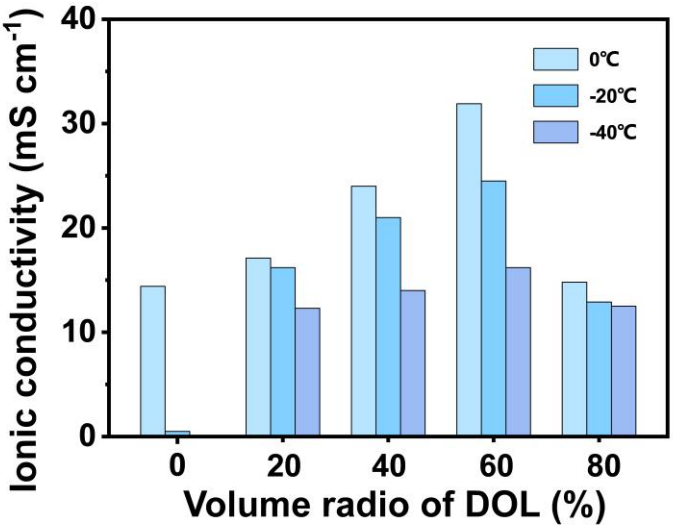

Figure S3. Comparison of ionic conductivity of the aqueous, BIS-$D_{0.2}$, BIS-$D_{0.4}$, BIS-$D_{0.6}$ and BIS-$D_{0.8}$ electrolytes at 0, -20 and -40°C.

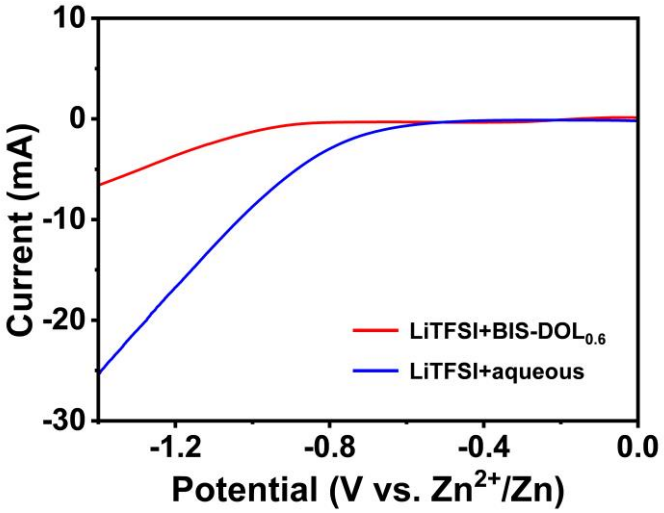

Figure S4. LSV profiles of Na_2SO_4 electrolyte with a scan rate of 5 mVs^{-1}.

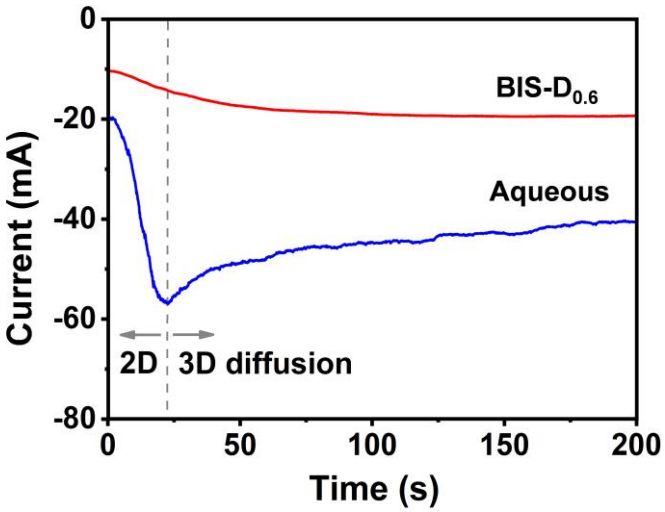

Figure S5. Chronoamperometric curves of Zn electrode deposition with aqueous and BIS-$D_{0.6}$ electrolytes under -150 mV.

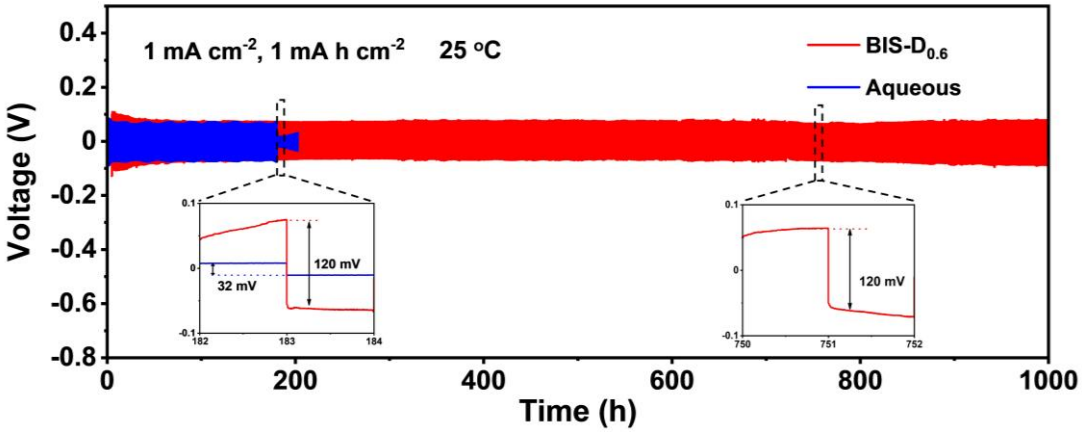

Figure S6. Long-term cycling of Zn||Zn symmetrical batteries at a current density of 1 mA cm^{-2} with a capacity of 1 mAh cm^{-2}. The small figures show the voltage distribution at different cycles at 25 °C.

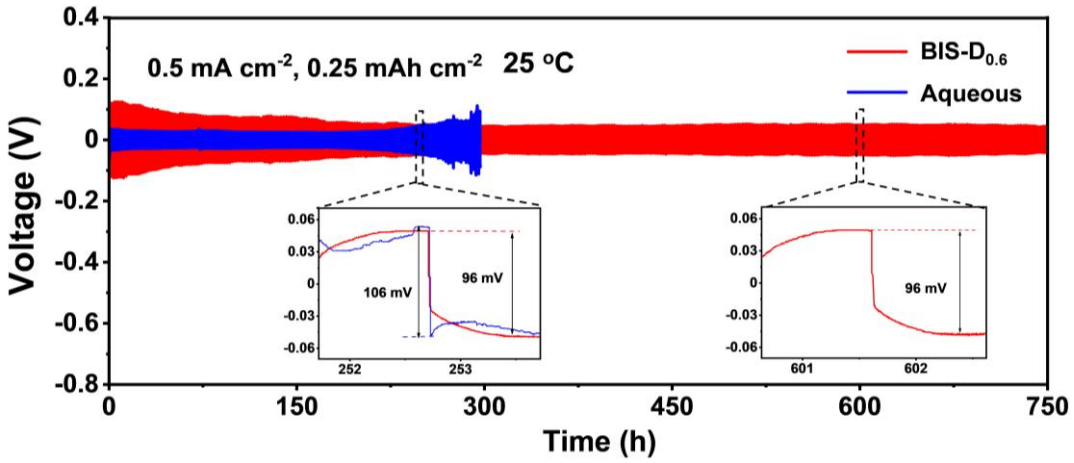

Figure S7. Long-term cycling of Zn||Zn symmetrical batteries at a current density of 0.5 mA cm^{-2} with a capacity of 0.25 mAh cm^{-2} at 25 °C.

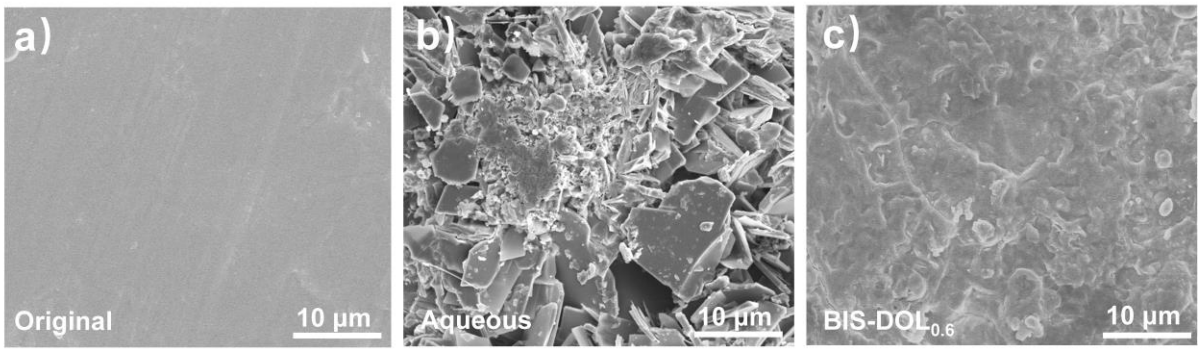

Figure S8. (a) SEM image of the original surface of Zn foil. SEM images of Zn deposition morphology for Zn||Zn batteries with (b) aqueous and (c) BIS-$D_{0.6}$ electrolytes after 50 cycles.

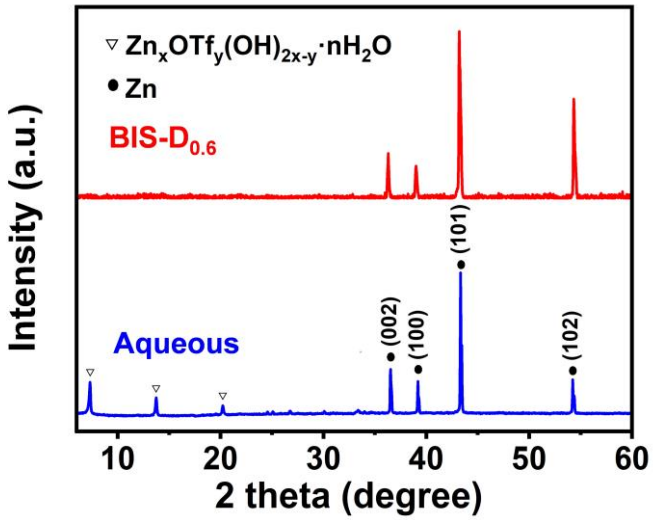

Figure S9. XRD patterns of Zn electrodes after 50 cycles with aqueous and BIS-$D_{0.6}$ electrolytes.

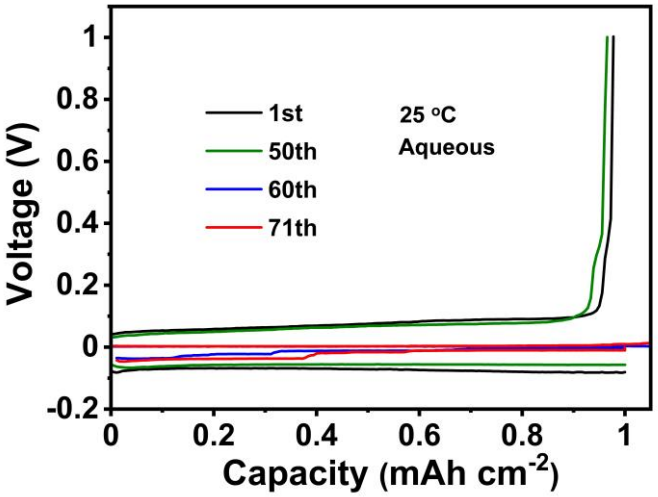

Figure S10. Voltage profiles of Zn||Cu asymmetric batteries using aqueous electrolyte at 25 °C.

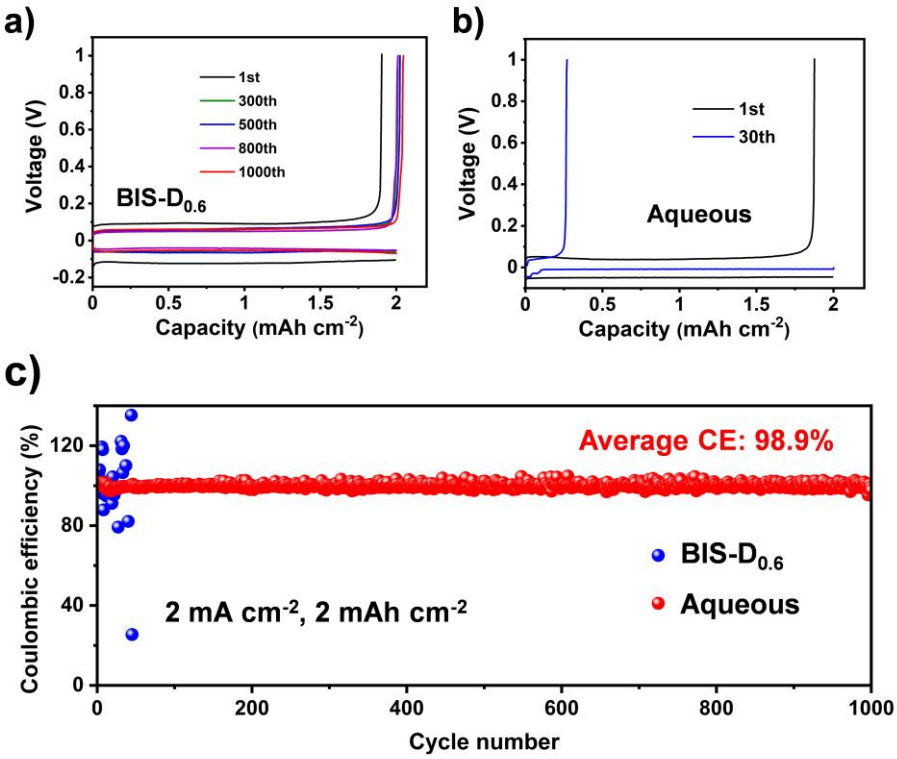

Figure S11. (a,b) Voltage profiles of Zn||Cu asymmetric batteries using BIS-$D_{0.6}$ and aqueous electrolytes at various cycles at 25 °C. (c) Cycling stability of Zn||Cu asymmetric batteries at 25 °C.

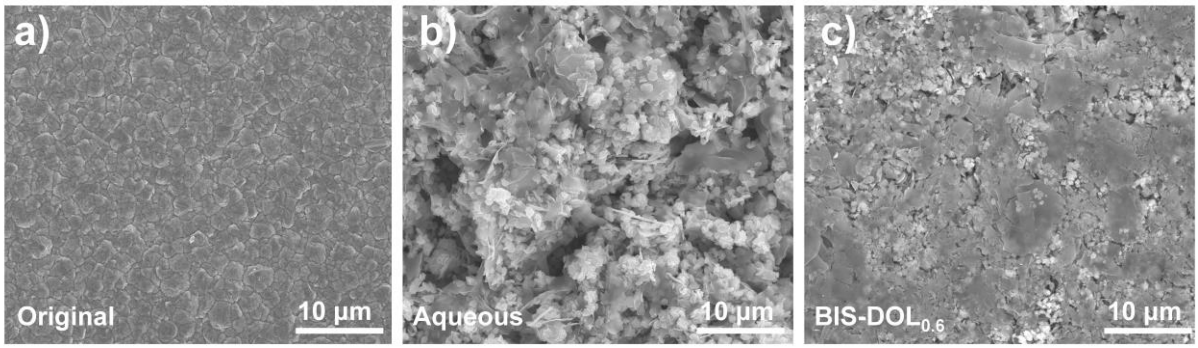

Figure S12. (a) SEM image of the original surface of Cu foil. SEM images of Cu surface morphology for Zn||Cu batteries with (b) aqueous and (c) BIS-$D_{0.6}$ electrolytes after 50 cycles.

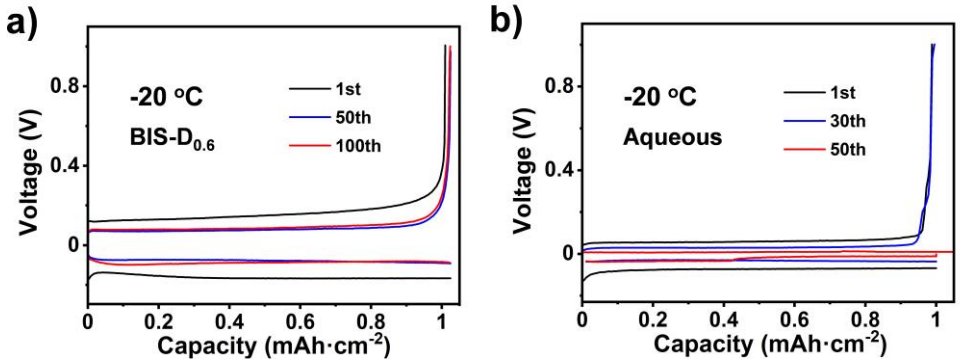

Figure S13. Voltage profiles of Zn||Cu asymmetric batteries using aqueous and BIS-$D_{0.6}$ electrolytes at -20 °C.

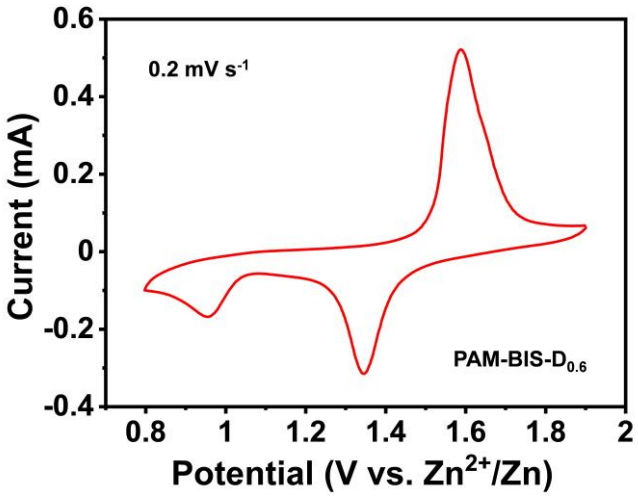

Figure S14. CV curves for Zn||MnO_2 batteries with the PAM-BIS-$D_{0.6}$ organohydrogel electrolyte at a scan rate of 0.2 mV s^{-1}.

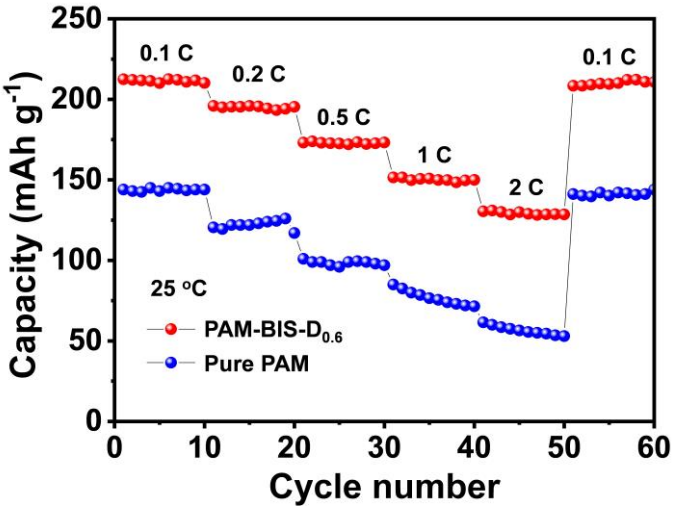

Figure S15. Rate performance of the batteries tested with the current densities varying from 0.1 to 2 C at 25 °C.

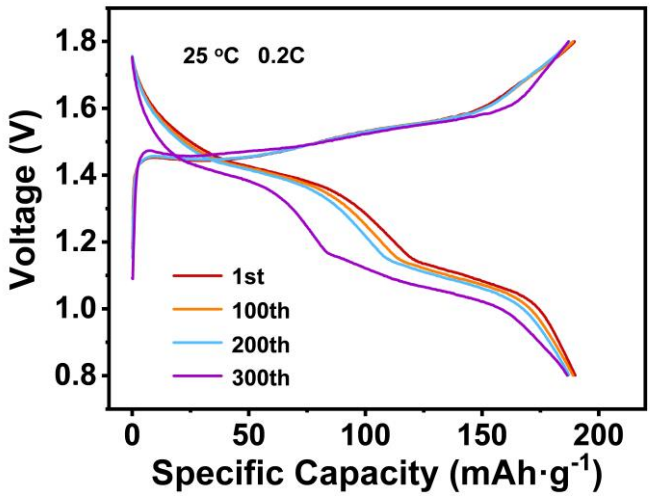

Figure 16. Charge/discharge curves with the PAM-BIS-$D_{0.6}$ organohydrogel electrolyte at 25 °C at 0.2C.

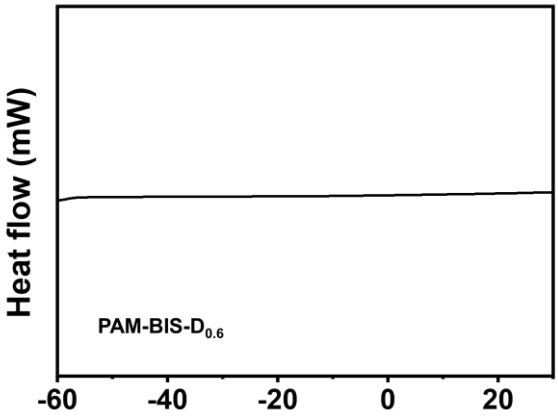

Figure S17. DSC curve for the PAM-BIS-$D_{0.6}$ organohydrogel electrolyte.

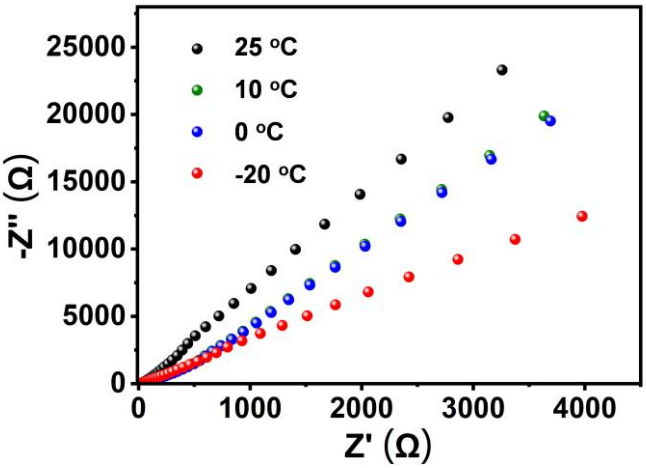

Figure S18. EIS plot of PAM-BIS-$D_{0.6}$ organohydrogel electrolyte at 25, 10, 0 and -20 °C.

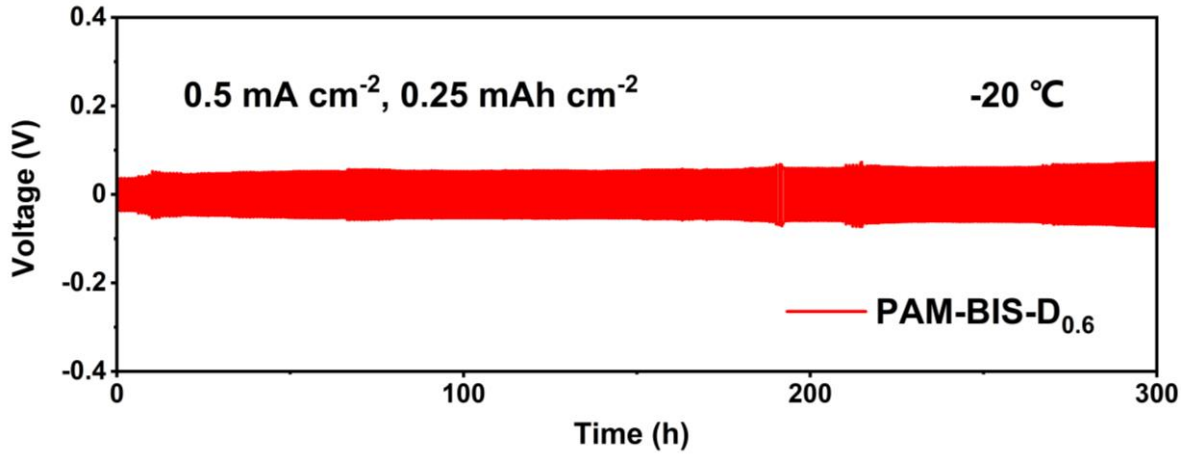

Figure S19. Long-term cycling of Zn||Zn symmetrical batteries with PAM-BIS-$D_{0.6}$ organohydrogel electrolyte at -20 °C.

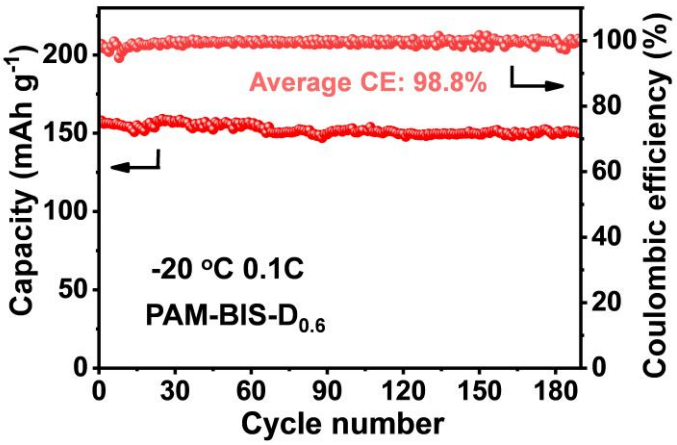

Figure S20. Cycling performance of Zn||PAM-BIS-$D_{0.6}$||MnO_2 batteries at the current density of 0.1C at -20 °C.

Table S1. Comparison of the Coulombic efficiency of Zn-Cu asymmetric batteries in aqueous electrolytes.

Electrolyte	Current density (mA cm^{-2})	Areal capacity (mAh cm^{-2})	CE(%)	Cycle number	References
1M $Zn(OTf)_2$+H_2O/DOL	**2**	**2**	**98.9**	**1000**	**This work**
1M $Zn(ClO_4)_2$+SN	**0.5**	**0.5**	**98.4**	**200**	**[S1]**
$Zn(ClO_4)_2$+ H_2O/MSM	**0.5**	**0.5**	**98**	**400**	**[S2]**
1M $ZnSO_4$ + 1000ppm CDA	**0.5**	**0.1**	**98**	**625**	**[S3]**
1M $Zn(OTf)_2$ +CH_3OH	**1**	**0.5**	**96.9**	**100**	**[S4]**
1M $Zn(OTf)_2$+H_2O/AN	**1**	**0.5**	**98.1**	**220**	**[S5]**
1M $Zn(TFSI)_2$+DMSO	**1**	**1**	**98.4**	**10**	**[S6]**

Video S1. The process of hydrogen evolution reactions with BIS-$D_{0.6}$ electrolyte.

Video S2. The process of hydrogen evolution reactions with aqueous electrolyte.

References

S1 W. Yang, X. Du, J. Zhao, Z. Chen, J. Li, J. Xie, Y. Zhang, Z. Cui, Q. Kong, Z. Zhao, C. Wang, Q. Zhang, G. Cui, *Joule* **2020**, 4, 1557–1574.

S2 M. Han, J. Huang, X. Xie, T. Li, J. Huang, S. Liang, J. Zhou, H. J. Fan, *Adv. Funct. Mater.* **2022**, 32, 2110957.

S3 M. Zhou, H. Chen, Z. Chen, Z. Hu, N. Wang, Y. Jin, X. Yu, H. Meng, *ACS Appl. Energy Mater.* **2022**, 5, 7590–7599.

S4 X. Lin, Z. Wang, L. Ge, J. Xu, W. Ma, M. Ren, W. Liu, J. Yao, C. Zhang, *ChemElectroChem.* **2022**, 9, e202101724.

S5 C. Meng, W. He, Z. Kong, Z. Liang, H. Zhao, Y. Lei, Y. Wu, X. Hao, *Chem. Eng. J.* **2022**, 450, 138265.

S6 Q. Jian, T. Wang, J. Sun, M. Wu, T. Zhao, *Energy Storage Mater.* **2022**, 53, 559–568.